Environmental Science

AIMS Environmental Science, 13(2): 331–347.
DOI: 10.3934/environsci.2026013
Received: 15 November 2025
Revised: 09 February 2026
Accepted: 06 March 2026
Published: 10 April 2026

https://www.aimspress.com/journal/environmental

Research article

CO_3^{2-} enhanced electron transfer and enzyme stabilization overcome the ion inhibition paradigm in aerobic denitrification

Jun Zhang[1,2,*], Tian Hu[2,3], Zhushuo Zhang[2,3], Yihang Ding[1], Chunling Zheng[1] and Shengtao Zhou[1]

[1] College of Water Resources and Modern Agriculture, Nanyang Normal University, Nanyang, 473061, China
[2] Collaborative Innovation Center of Water Security for the Water Source Region of Mid-line of the South-to-North Diversion Project of Henan Province, Nanyang Normal University, Nanyang, 473061, China
[3] College of Life Sciences, Nanyang Normal University, Nanyang, 473061, China

* **Correspondence:** Email: zhangjun0993@163.com; Tel: +037763513567.

Abstract: Aerobic denitrifying bacteria are often inhibited by inorganic ions during wastewater treatment, and elucidating their regulatory mechanisms is crucial for enhancing nitrogen removal efficiency. In this study, we systematically investigated the effects of varying concentrations of inorganic ions (0–200 mg/L) on the growth, denitrification performance, and metabolic activity of *Pseudomonas mosselii* H6. Based on enzyme kinetics, energy metabolism indicators, and measurements of electron transport chain activity, CO_3^{2-} was found to significantly enhance denitrification capacity. At 200 mg/L, electron transport system activity (ETSA) increased by 26.42%, ATP synthesis peaked at 1.25 μmol/mg prot, and the NADH/NAD^+ ratio rose to 22.69. Nitrate reductase (NR) and nitrite reductase (NiR) activities reached 28.37 and 17.76 U/mg prot, respectively. In contrast, Cl^- and NO_3^- at 200 mg/L markedly suppressed cellular metabolism, reducing NH_4^+-N removal efficiency to 21.41% and 16.42%, respectively. These findings revealed a concentration-dependent and ion-specific regulatory mechanism. CO_3^{2-} enhances nitrogen removal by optimizing electron transfer and improving enzyme stability. This study provides a theoretical foundation for optimizing the biological treatment of high-salinity wastewater.

Keywords: aerobic denitrification; *Pseudomonas mosselii* H6; CO_3^{2-}; electron transport; enzyme stability

1. Introduction

Industrial processes and human activities have led to a sharp increase in the discharge of high ammonia nitrogen wastewater [1]. It has been established that excessive discharge of ammonia nitrogen leads to eutrophication of water bodies, which is a serious threat to ecological balance [2]. High ammonia nitrogen wastewater has become an urgent problem, emphasizing the need to develop prevention strategies. In recent years, heterotrophic nitrification-aerobic denitrification (HN-AD) bacteria have emerged as efficient denitrifying microorganisms, overcoming limitations of conventional biological nitrogen removal processes [3,4]. HN-AD bacteria perform simultaneous nitrification and denitrification under aerobic conditions [5]. This capability enables them to remove nitrogen and carbon concurrently while minimizing greenhouse gas emissions [6].

Biological treatment technologies have gained prominence in high-salinity organic wastewater treatment due to their environmental compatibility and cost-effectiveness, surpassing traditional physical-chemical methods [7]. However, real wastewater often contains complex inorganic ions (e.g., Cl^-, NO_3^-, and SO_4^{2-}). These ions can inhibit aerobic denitrification through multiple pathways: (1) Inducing osmotic stress [8,9], (2) suppressing enzyme activity[10], or (3) disrupting electron transport efficiency [11]. Researchers have identified specific inhibitory mechanisms. For example, high Cl^- concentrations damage cell membrane integrity [12], while NO_3^- competitively occupies enzyme active sites [13]. Although most salt ions negatively impact microbial activity, their effects vary depending on ion type and concentration. Thus, elucidating the mechanisms of ion-specific inhibition is critical for optimizing treatment strategies for high-ammonia-nitrogen wastewater. These gaps underscore the need for targeted research.

Studies suggest that carbonate-like ions (HCO_3^-/CO_3^{2-}) play a dual role in microbial metabolism [14,15]: On the one hand, the alkaline property regulates intracellular pH and mitigates the accumulation of acidic metabolites, H^+ produced during denitrification [16]; on the other hand, CO_3^{2-} may act as a cofactor involved in the stability maintenance of metalloenzymes, stabilizing the 4Fe-4S cluster of nitrate reductase [17]. However, these hypotheses have not been systematically verified in aerobic denitrification systems, especially the regulatory pathways of CO_3^{2-} on electron transport chain activity (ETSA) and energy metabolism remain unclear. In addition, most researchers have focused on the low concentration ion effect (≤ 100 mg/L) [18], while the mechanism of high concentration (200 mg/L) alkaline ions on the nitrogen removal performance of the strain needs to be resolved urgently.

In this study, we systematically investigate the effects of varying CO_3^{2-} concentrations (0–200 mg/L) on the growth, denitrification performance, and key metabolic activities of the efficient aerobic denitrifier *Pseudomonas mosselii* H6, with comparative analyses of HCO_3^-, Cl^-, SO_4^-, and NO_3^-. Through integrated analyses of enzyme kinetics (NR, NiR, NOR, N_2OR), energy metabolism parameters (ATP, NADH/NAD^+ ratio), and electron transport chain activity, we demonstrate, for the first time, that CO_3^{2-} enhances denitrification through dual mechanisms: (1) Optimizing electron transfer efficiency and (2) stabilizing denitrifying enzymes. These findings provide novel insights into the unique role of alkaline ions in microbial metabolism and establish a theoretical foundation for optimizing biological treatment processes for high-salinity wastewater. Specifically, our results suggest that carbonate buffers (e.g., Na_2CO_3) could be strategically employed to mitigate the inhibitory effects of Cl^-/NO_3^- in wastewater treatment systems

2. Materials and methods

2.1. Bacterial strain and medium

The bacterial strain *Pseudomonas mosselii* H6 used in this study was isolated from activated sludge in sewage treatment plants [19]. The denitrification medium (DM) used for bacteria cultivation and performance evaluation contained (per liter) $C_6H_{12}O_6$ 4.86 g, $Na_2HPO_4{\cdot}7H_2O$ 7.9 g, KNO_3 1.0 g, KH_2PO_4 1.5 g, NH_4Cl 0.3 g, $MgSO_4{\cdot}7H_2O$ 0.1 g, and 0.1 mL trace element solution. The medium was adjusted to pH 7.0–7.2 and autoclaved for sterility at 121 °C for 20 min.

2.2. The influences of CO_3^{2-}, HCO_3^-, Cl^-, and NO_3^- on nitrogen removal of strain H6

To evaluate the impacts of various inorganic ions (CO_3^{2-}, HCO_3^-, Cl^-, and NO_3^-) on nitrogen removal of strain H6, pre-cultured strain H6 was inoculated (1%, v/v) into DM containing different ions. The ions concentrations were set at 0, 50, 100, 150, and 200 mg/L, respectively. All media were cultivated in a shaker (180 rpm for 24 h at 30 °C). Media samples were collected every 4 h, and OD_{600} was determined immediately. The remaining samples were centrifuged (8,000 rpm for 5 min at 4 °C), and the supernatant was used to determine the concentrations of NH_4^+-N, NO_3^--N and NO_2^--N. All experiments were carried out in triplicate.

2.3. Influence mechanisms of CO_3^{2-}, HCO_3^-, Cl^-, and NO_3^- on the aerobic denitrification processes of strain H6

To explore the influence mechanism of CO_3^{2-}, HCO_3^-, Cl^-, and NO_3^- on the aerobic denitrification processes of strain H6, the concentrations of NADH, NAD^+, ATP, and the activities of NR, NiR, NOR, and N_2OR, as well as ETSA at different growth stages were determined under the ion concentrations of 0, 50, 100, 150, and 200 mg/L. In the experiments, carbon source, shaking speed, temperature, and pH were glucose, 180 rpm, 30 °C, and 7.0 respectively. The experiments were carried out for 24 h, and samples were taken every 4 h.

2.4. Analytical methods

2.4.1. Determination of cell growth and nitrogen compounds

The OD_{600} was monitored by measuring the absorbance of the cultivated medium at 600 nm with a spectrophotometer (Puxi TU-1900, Henan). NH_4^+-N, NO_3^--N, and NO_2^--N concentrations were measured at wavelengths of 420 nm, 220 & 275 nm, and 520 nm, respectively, using the National Standard Methods of the People's Republic of China after centrifugation at 8,000 rpm for 5 min.

2.4.2. Determination of NADH, NAD^+, ETSA, ATP, and enzyme activity

ATP, NADH, NAD^+, protein content, and NR and NiR activities were determined by assay kits (Beijing Boxbio Science & Technology Co., Ltd, China), and NOR and N_2OR activities were determined by ELISA kits Shanghai Baililai Biotechnology Co., Ltd, China). The operation methods

were strictly in accordance with the adherence to the kits' instructions.

Intracellular ATP, NADH, and NAD^+ concentrations were determined using commercial assay kits (Beijing Boxbio Science & Technology Co., Ltd, China). For ATP measurement, the luciferase-based bioluminescence method was employed. Briefly, cell pellets collected by centrifugation (8,000 rpm, 5 min, 4 °C) were lysed with the provided extraction buffer on ice for 15 min. After centrifugation (12,000 rpm, 10 min, 4 °C), the supernatant was mixed with the luciferase reagent, and luminescence was measured immediately using a microplate reader (wavelength not required for luminescence). The ATP concentration was calculated based on a standard curve and normalized to the total protein content of the lysate.

For NADH and NAD^+, the assays were based on enzymatic cycling reactions that convert a precursor to a colored product proportional to the cofactor concentration. Cell extracts were prepared similarly, and aliquots were treated to measure either total NAD(H) or NAD^+ alone (after decomposing NADH at 60 °C for 30 min). NADH concentration was obtained by subtraction. Absorbance was read at 450 nm for NADH and 570 nm for NAD^+, and concentrations were calculated using kit-provided standards and normalized to protein content.

Enzyme activities of NR, NiR, NOR, and N_2OR were determined using cell-free extracts. Cells were harvested by centrifugation, washed twice with phosphate buffer (50 mM, pH 7.4), and disrupted by sonication on ice (5 cycles of 10 s pulse with 20 s intervals). The homogenate was centrifuged (12,000 rpm, 20 min, 4 °C), and the supernatant was used as the crude enzyme extract. Protein concentration was determined using the Bradford method.

Nitrate reductase (NR) and nitrite reductase (NiR) activities were measured using assay kits (Beijing Boxbio). For NR, the reaction mixture contained the enzyme extract, NADH, and KNO_3 in phosphate buffer. The decrease in nitrite concentration (as an intermediate product stabilized and quantified colorimetrically) over 30 min at 30 °C was monitored at 540 nm. One unit (U) of NR activity was defined as the amount of enzyme that catalyzes the reduction of 1 μmol NO_3^- per minute per mg protein. For NiR, the assay similarly measured the disappearance of NO_2^- in the presence of reduced methyl viologen as an electron donor, with absorbance measured at 540 nm after a 20 min incubation at 30 °C.

Nitric oxide reductase (NOR) and nitrous oxide reductase (N_2OR) activities were determined using sandwich ELISA kits (Shanghai Baililai Biotechnology Co., Ltd, China). Microwell plates pre-coated with anti-NOR or anti-N_2OR antibodies were incubated with the crude enzyme extract at 37 °C for 1 h. After washing, a biotin-conjugated detection antibody was added, followed by streptavidin-HRP and TMB substrate. The reaction was stopped with H_2SO_4, and absorbance was measured at 450 nm. Enzyme activity (U/mL) was interpolated from a standard curve generated with purified NOR or N_2OR protein provided in the kit.

The ETSA was determined by the reduction of the electron acceptor 2-(p-iodophenyl)-(p-nitrophenyl) 5-phenyl tetrazolium chloride (INT) to formazan (INF) at the end of the experiment [20]. Then, 2 mL of INT (0.2%) was added to 1 mL suspension samples collected from serum bottles and incubated at 25 °C for 20 min in the dark, after which 0.2 mL methanol of formaldehyde was added to the mixture as the termination agent. Subsequently, the cells were harvested from the samples by centrifugation at 10,000 rpm for 5 min, and then 4 mL of 96% methanol was used to extract the INF. Finally, the mixed INF extract was measured by a spectrophotometer (Puxi TU-1900, Henan) at 495 nm. The ETSA was calculated according to the following formula:

$$[\,ETSA(\mathrm{ug}O_2 g^{-1}\min^{-1}) = \frac{Ab \times V \times 32}{15.9 \times 2 \times S \times t}\,] \quad (1)$$

where Ab is the sample absorbance at 495 nm, V and S are the initial volume of sample and the total volume of methanol (mL), respectively, and 32/2 is the constant transformed from INT-formazan (μmol) to O_2 (μg). The value 15.9 is the special absorption coefficient of INT-formazan, and t is the incubation time (min).

2.5. Statistical analysis

All experiments were repeated three times, and the data were expressed as mean±SD. Statistical significance among experimental groups was analyzed using one-way analysis of variance (ANOVA), followed by Tukey's post hoc test for multiple comparisons. For data statistics and analysis, IBM SPSS Statistics 27.0 was employed, whereas Origin 2023 was utilized for mapping purposes.

3. Results

3.1. Effects of $CO3^{2-}$, HCO^{3-}, Cl^{-}, and NO^{3-} on nitrogen removal of strain H6

The growth of strain H6 exhibited a clear concentration-dependent response to CO_3^{2-}, HCO_3^{-}, Cl^{-}, and NO_3^{-} (Figure 1). Under low-concentration conditions, these ions had limited effects on bacterial growth, and the OD_{600} values gradually increased and stabilized within 24 h. When the ion concentrations increased to 200 mg/L, bacterial growth was inhibited to varying degrees, as indicated by a general decline in OD_{600} values. The inhibitory effects of Cl^{-} and NO_3^{-} were more pronounced, with OD_{600} values of 1.83 and 1.93, representing decreases of 10.07% and 5.36% compared with the control. The inhibitory effects of CO_3^{2-} and HCO_3^{-} were relatively weak.

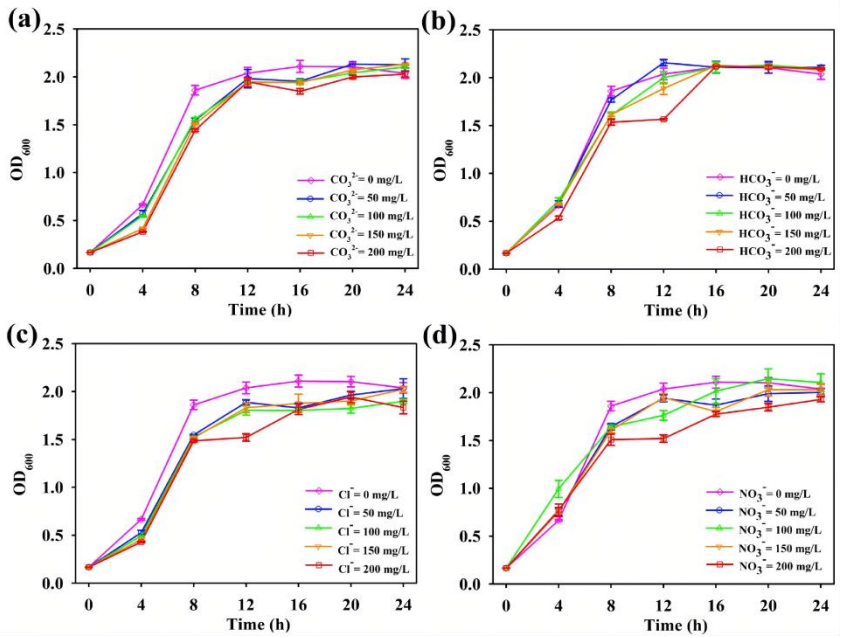

Figure 1. Effect of ions on the growth of strain H6 ((a): CO_3^{2-}; (b): HCO_3^{-}; (c): Cl^{-}; and (d): NO_3^{-}).

The NH_4^+-N removal efficiency declined significantly with increasing ion concentrations (Figure 2). At 50 mg/L, the treatments with CO_3^{2-}, HCO_3^-, Cl^-, and NO_3^- showed relatively high removal efficiencies, reaching 45.53%, 47.95%, 32.37%, and 30.05%, respectively. When the ion concentration increased to 200 mg/L, a marked decrease in NH_4^+-N removal was observed. Cl^- and NO_3^- exhibited the strongest inhibitory effects, reducing the removal efficiencies to 21.41% and 16.42%, respectively (Figure S1).

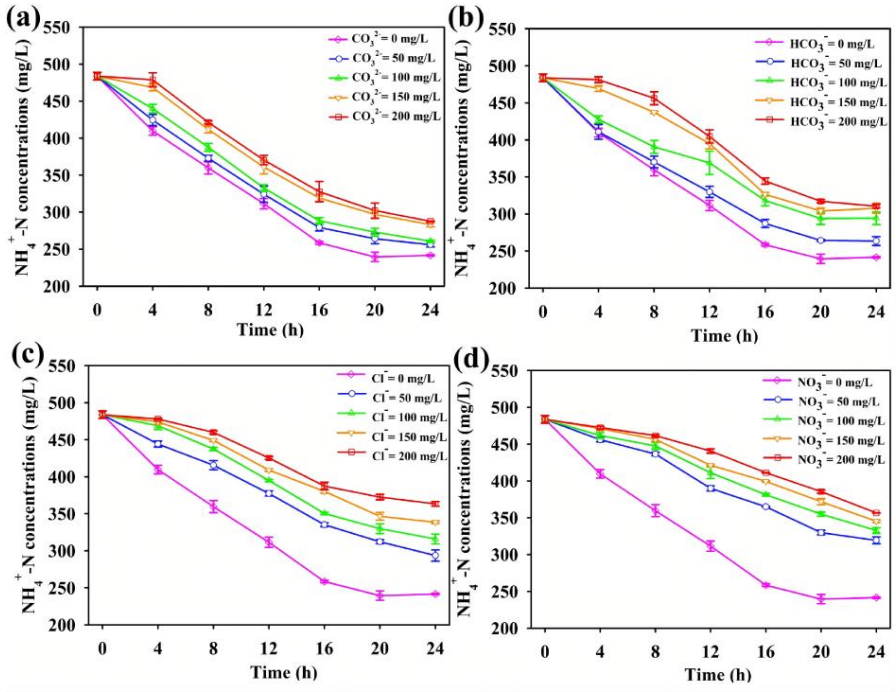

Figure 2. Effect of ions on the removal of NH_4^+-N by strain H6 ((a): CO_3^{2-}; (b): HCO_3^-; (c): Cl^-; and (d): NO_3^-).

The NO_3^--N reduction rate exhibited a rise-and-fall pattern in response to increasing ion concentrations (Figure 3). HCO_3^- and Cl^- showed the most pronounced stimulatory effects at 150 mg/L, with maximum reduction rates of 55.35 and 66.61 $mg \cdot L^{-1} \cdot h^{-1}$, respectively. However, at 200 mg/L, both ions exerted inhibitory effects, and the reduction rate under HCO_3^- treatment declined sharply to 14.33 $mg \cdot L^{-1} \cdot h^{-1}$. In contrast, CO_3^{2-} consistently enhanced NO_3^--N reduction, reaching a peak value of 59.53 $mg \cdot L^{-1} \cdot h^{-1}$ at 200 mg/L. Variations in the external NO_3^- concentration had a relatively minor impact on the reduction rate, with only slight increases observed at 100 and 150 mg/L, yielding rates of 47.08 and 24.44 $mg \cdot L^{-1} \cdot h^{-1}$, respectively (Figure S2).

The NO_2^--N reduction rate exhibited a distinct increase followed by a decline as ion concentrations increased (Figure 4). When the concentrations of HCO_3^- and Cl^- increased from 50 mg/L to 150 mg/L, the corresponding reduction rates rose from 85.42 to 140.06 $mg \cdot L^{-1} \cdot h^{-1}$ and from 220.55 to 250.30 $mg \cdot L^{-1} \cdot h^{-1}$, respectively. However, at 200 mg/L, a decrease in reduction rates was observed for all three ions. In contrast, CO_3^{2-} continuously promoted NO_2^--N reduction, with the highest rate of 241.16 $mg \cdot L^{-1} \cdot h^{-1}$ recorded at 200 mg/L. Additionally, variations in exogenous NO_3^- concentration significantly affected the NO_2^--N reduction rate, with a marked increase at 100 mg/L, reaching a peak of 273.23 $mg \cdot L^{-1} \cdot h^{-1}$ (Figure S3).

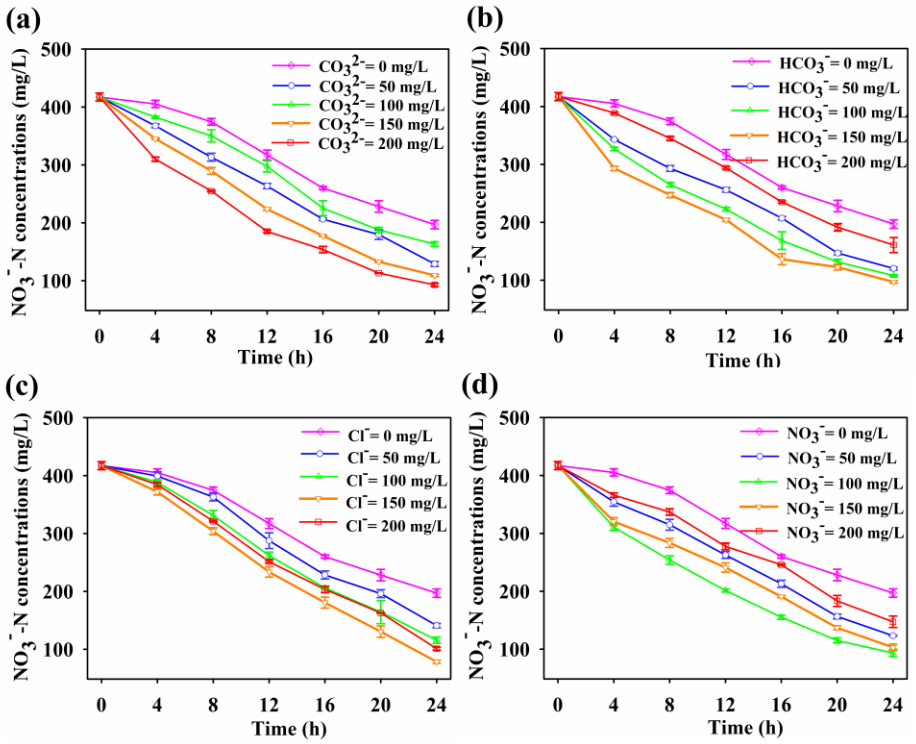

Figure 3. Effect of ions on the removal of H6 NO_3^--N by strain H6 ((a): CO_3^{2-}; (b): HCO_3^-; (c): Cl^-; and (d): NO_3^-).

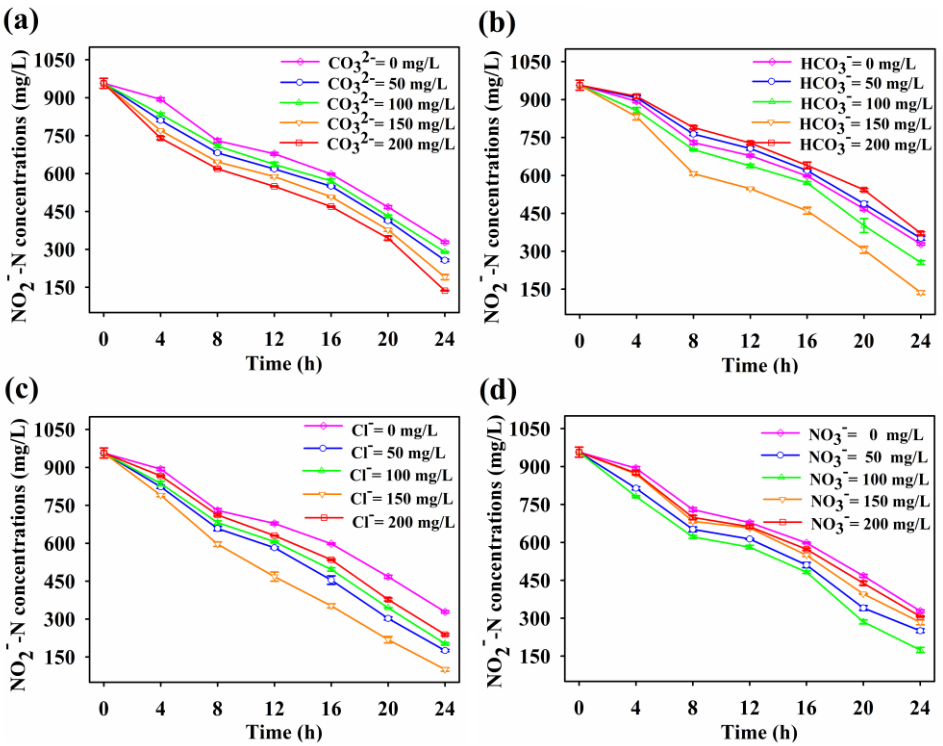

Figure 4. Effect of ions on the removal of H6 NO_2^--N by strain H6 ((a): CO_3^{2-}; (b): HCO_3^-; (c): Cl^-; and (d): NO_3^-).

3.2. *Effects of CO_3^{2-}, HCO_3^-, Cl^-, and NO_3^- on aerobic denitrifying enzyme activity of strain H6*

The NR activity of strain H6 exhibited a distinct "low-concentration stimulation and high-concentration inhibition" pattern with increasing ion concentrations (Figure 5). HCO_3^- and Cl^- showed the most pronounced enhancement at 150 mg/L, with NR activities reaching 23.29 and 31.52 U/mg prot, respectively, but both declined significantly at 200 mg/L. In contrast, CO_3^{2-} exerted a concentration-dependent stimulatory effect, with NR activity increasing steadily from 16.39 U/mg prot at 50 mg/L to 28.37 U/mg prot at 200 mg/L. Exogenous NO_3^- also induced a biphasic response, with NR activity peaking at 18.69 U/mg prot at 100 mg/L and decreasing to 12.40 U/mg prot at 200 mg/L.

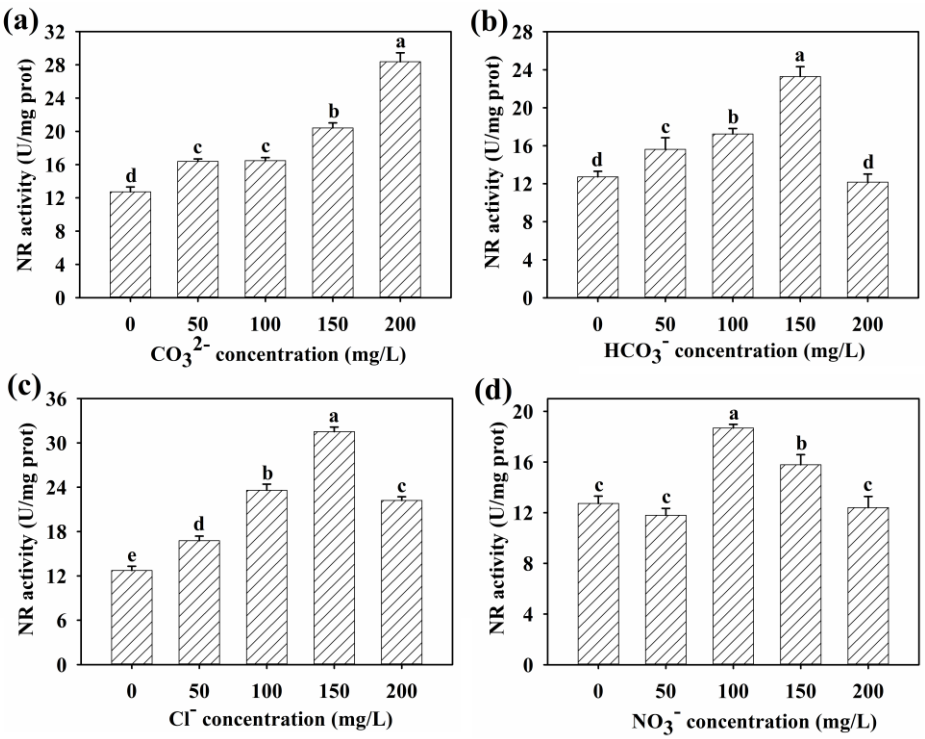

Figure 5. Effect of ions on the NR activity of strain H6 ((a): CO_3^{2-}; (b): HCO_3^-; (c): Cl^-; and (d): NO_3^-).

The NiR activity of strain H6 exhibited a concentration-dependent pattern, with an initial increase followed by a decline (Figure 6). The most significant enhancement was observed at 150 mg/L for HCO_3^- and Cl^-, with NiR activities reaching 15.63 and 18.18 U/mg prot, respectively; however, at 200 mg/L, the activity significantly decreased to 9.26 and 8.42 U/mg prot. In contrast, CO_3^{2-} consistently promoted NiR activity across the concentration range, peaking at 17.76 U/mg prot at 200 mg/L. Exogenous NO_3^- also exhibited a concentration-dependent effect on NiR activity, reaching a maximum of 18.46 U/mg prot at 100 mg/L, and decreasing to 9.30 U/mg prot at 200 mg/L.

The NOR activity of strain H6 exhibited a concentration-dependent response to CO_3^{2-}, HCO_3^-, Cl^-, and NO_3^-, with notable differences in trends among the ions (Figure 7). At low concentrations, CO_3^{2-} and Cl^- significantly enhanced NOR activity. However, when the concentration reaches 150 mg/L, NOR activity decreased to its lowest levels of 0.75 U/mL and 0.70 U/mL, respectively, before increasing slightly at 200 mg/L. HCO_3^- consistently inhibited NOR activity across all concentrations, with the lowest activity of 0.73 U/mL observed at 150 mg/L. The effect of NO_3^- on NOR activity followed a "low stimulation, high inhibition" pattern, significantly promoting activity at 50 mg/L, but

causing a marked decline in activity at concentrations of 150 mg/L and above. NOR activity reached its lowest value at 150 mg/L.

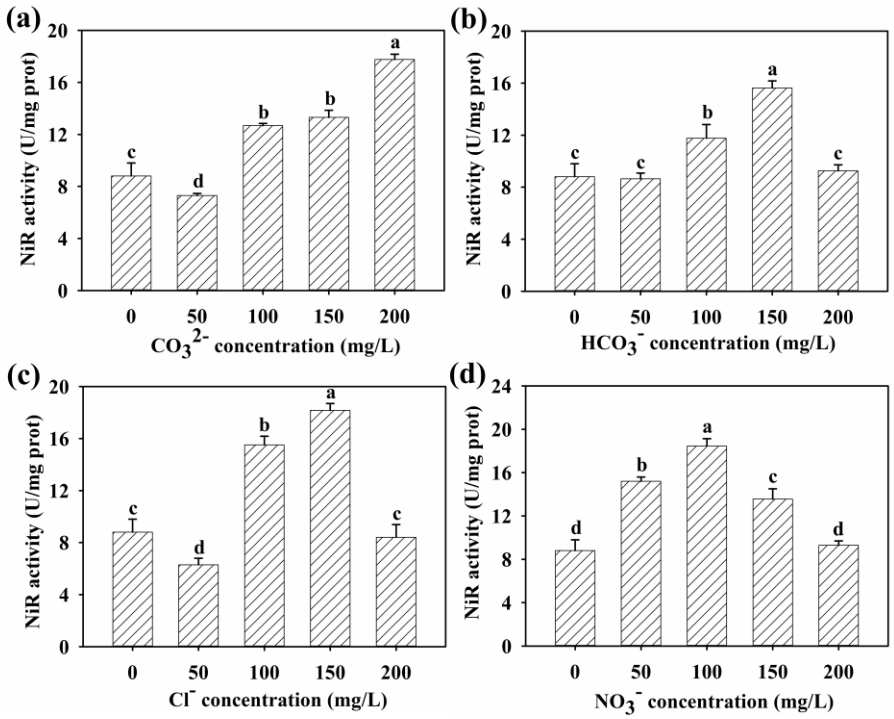

Figure 6. Effect of ions on the NiR activity of strain H6 ((a): CO_3^{2-}; (b): HCO_3^-; (c): Cl^-; and (d): NO_3^-).

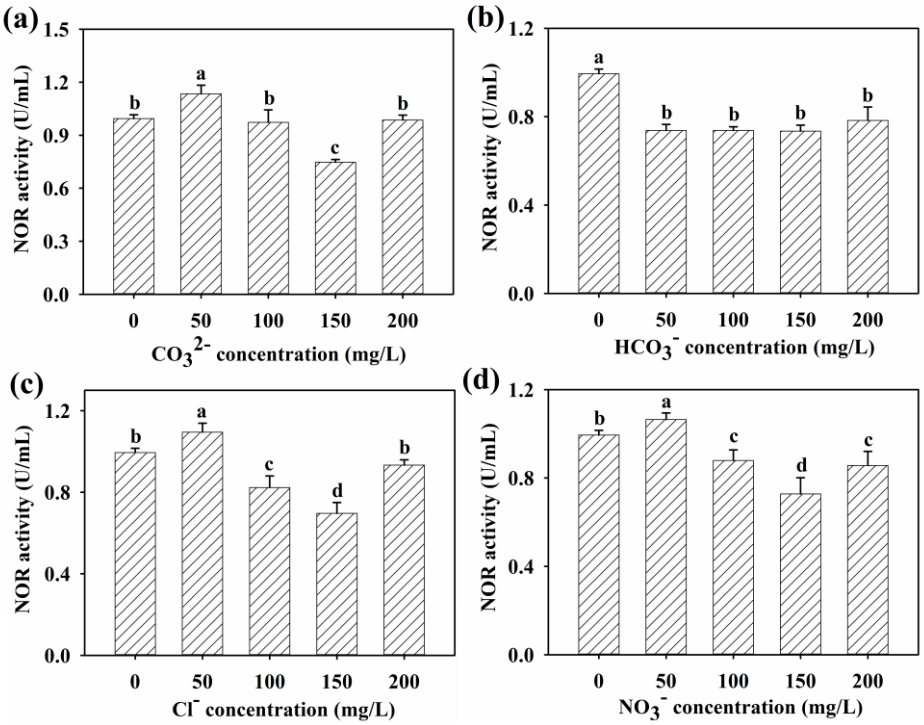

Figure 7. Effect of ions on the NOR activity of strain H6 ((a): CO_3^{2-}; (b): HCO_3^-; (c): Cl^-; and (d): NO_3^-).

The N_2OR activity of strain H6 exhibited significant concentration dependence and ion specificity in response to CO_3^{2-}, HCO_3^-, Cl^-, and NO_3^- (Figure 8). At 50 mg/L, all ions significantly enhanced N_2OR activity, reaching peak values of 1.68, 1.97, 1.70, and 1.70 U/mL, respectively. However, at concentrations of 150 mg/L, HCO_3^- and Cl^- inhibited N_2OR activity, reducing it to 1.46 and 1.42 U/mL. In contrast, NO_3^- consistently promoted N_2OR activity, maintaining elevated enzyme activity levels within the 50–200 mg/L range.

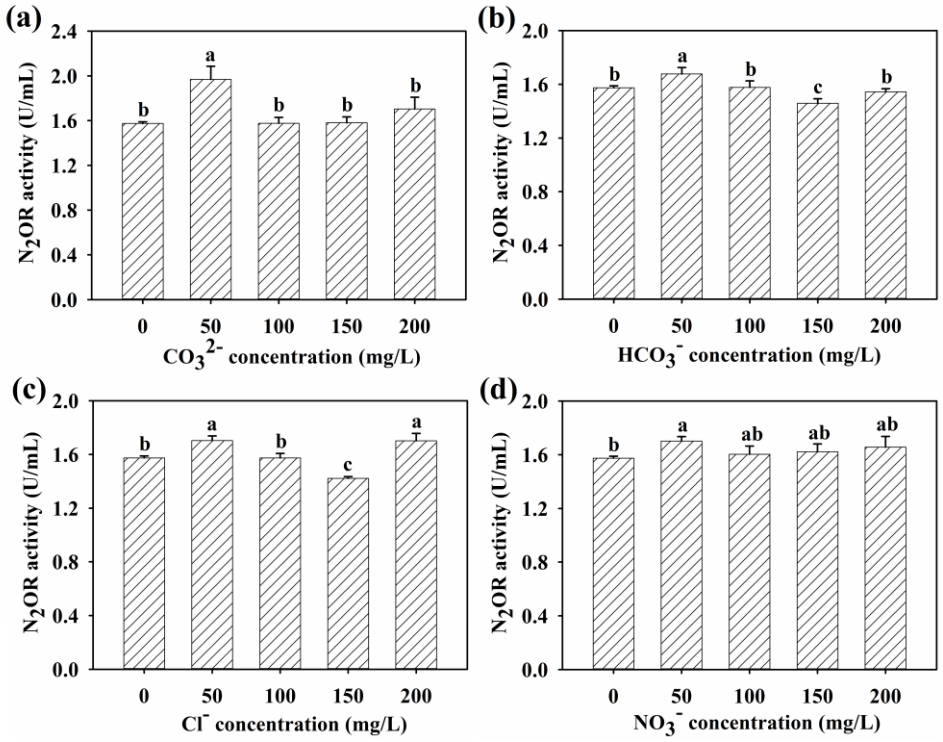

Figure 8. Effect of ions on the N_2OR activity of strain H6 ((a): CO_3^{2-}; (b): HCO_3^-; (c): Cl^-; and (d): NO_3^-).

3.3. Effects of CO_3^{2-}, HCO_3^-, Cl^-, and NO_3^- on ATP, NADH/NAD$^+$ and ETSA of strain H6

The ATP content of strain H6 exhibited significant concentration-dependent regulation in response to CO_3^{2-}, HCO_3^-, Cl^-, and NO_3^- (Figure 9). Under 150 mg/L conditions, ATP content peaked in the HCO_3^- and Cl^- treatment groups, reaching 2.76 and 1.28 μmol/mg prot, respectively. However, at 200 mg/L, ATP content significantly decreased to 1.15 and 0.90 μmol/mg prot. CO_3^{2-} continuously promoted an increase in ATP content with rising concentrations, peaking at 1.25 μmol/mg prot at 200 mg/L. The effect of NO_3^- on ATP content followed a "increase then decrease" trend, with a maximum of 2.30 μmol/mg prot observed at 100 mg/L.

The NADH/NAD$^+$ ratio of the strain exhibited significant concentration-dependent regulation in response to CO_3^{2-}, HCO_3^-, Cl^-, and NO_3^- (Figure 10). Under HCO_3^- and Cl^- treatments, the NADH/NAD$^+$ ratio reached its highest values at 150 mg/L, with values of 10.41 and 13.79, respectively. However, at 200 mg/L, the NADH/NAD$^+$ ratio significantly decreased to 5.10 and 5.14. CO_3^{2-} continuously increased the NADH/NAD$^+$ ratio with rising concentrations, peaking at 22.69 at 200 mg/L. In contrast, the effect of NO_3^- on the NADH/NAD$^+$ ratio was relatively minor, with a significant increase observed only at 100 mg/L, where it reached a max of 7.42.

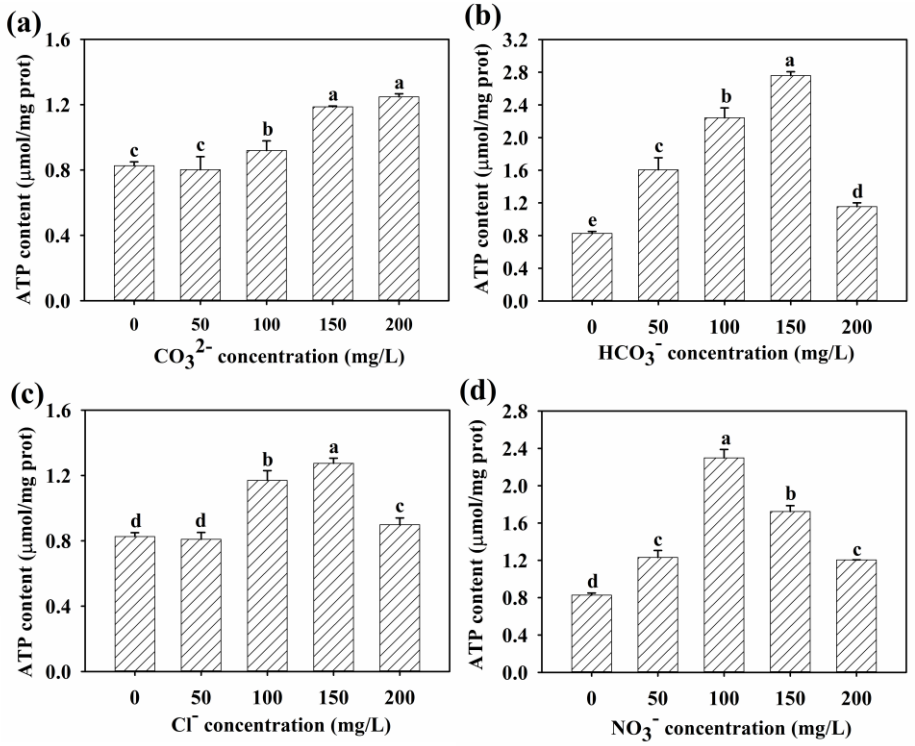

Figure 9. Effect of ions on the ATP content of strain H6 ((a): CO_3^{2-}; (b): HCO_3^-; (c): Cl^-; and (d): NO_3^-).

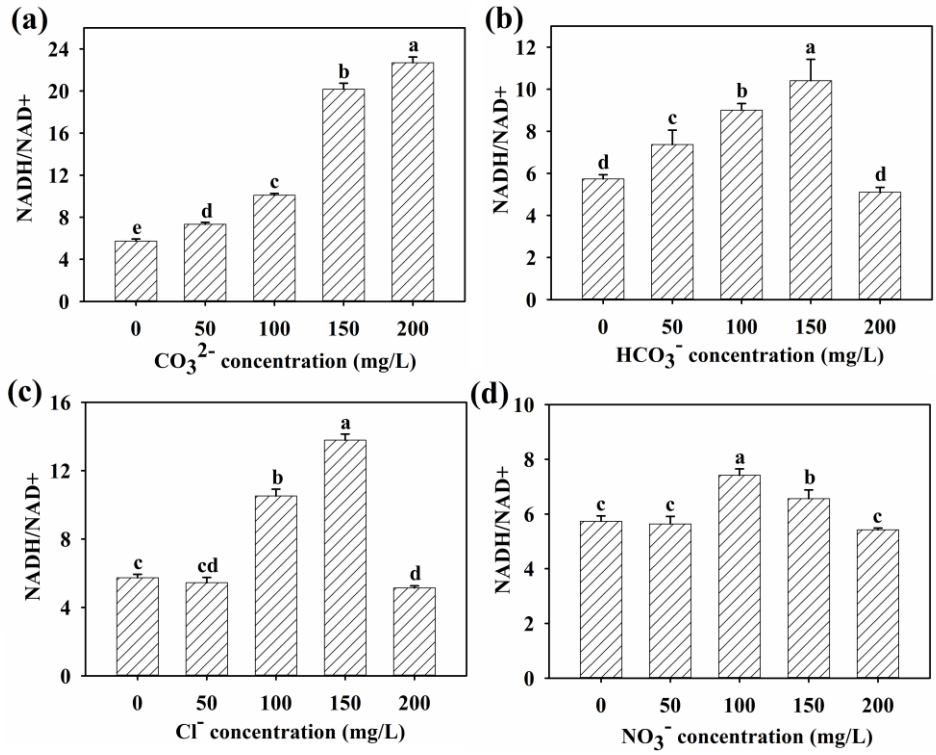

Figure 10. Effect of ions on the NADH/NAD^+ of strain H6 ((a): CO_3^{2-}; (b): HCO_3^-; (c): Cl^-; and (d): NO_3^-).

The effect of CO_3^{2-}, HCO_3^-, Cl^-, and NO_3^- on the ETSA activity of strain H6 was concentration-dependent (Figure 11). HCO_3^- had no significant effect on the ETSA activity of the strain. In contrast, increasing concentrations of CO_3^{2-} significantly enhanced ETSA activity, with a peak value of 0.014 $\mu g \cdot O_2 \cdot g^{-1} \cdot min^{-1}$ observed at 200 mg/L. Additionally, Cl^- and NO_3^- exhibited a "low stimulation, high inhibition" trend in their effects on ETSA activity. The maximum ETSA activity for Cl^- was 0.013 $\mu g \cdot O_2 \cdot g^{-1} \cdot min^{-1}$ at 150 mg/L, while NO_3^- reached its peak value of 0.014 $\mu g \cdot O_2 \cdot g^{-1} \cdot min^{-1}$ at 100 mg/L.

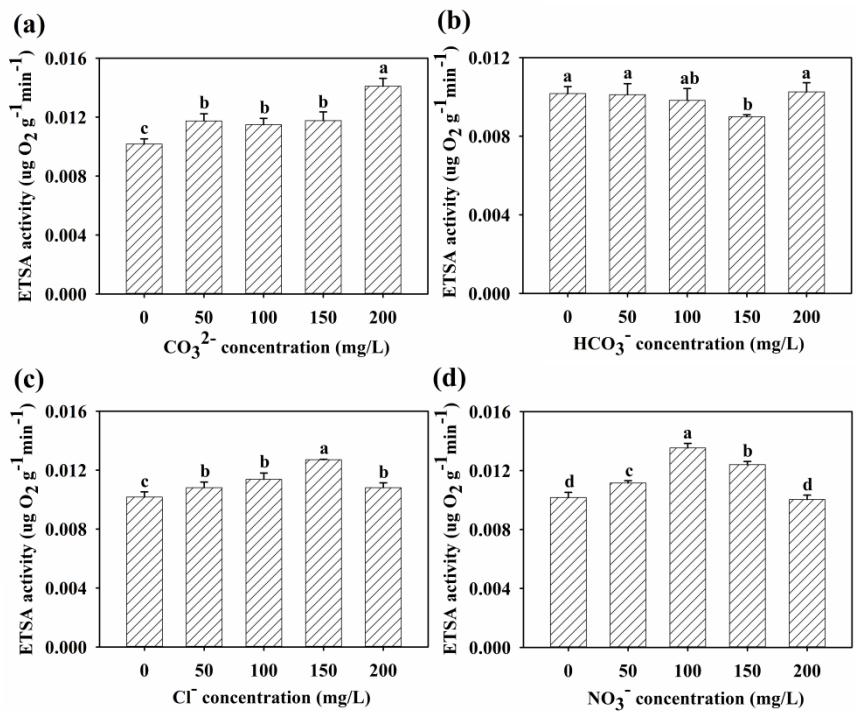

Figure 11. Effect of ions on the ETSA activity of strain H6 ((a): CO_3^{2-}; (b): HCO_3^-; (c): Cl^-; and (d): NO_3^-).

4. Discussion

The significant optimization of the electron transport chain (ETC) by CO_3^{2-} is a core driver for improving the denitrification efficiency of strain H6. Under 200 mg/L CO_3^{2-} treatment, the ETSA activity of strain H6 reached 0.014 $\mu g \cdot O_2 \cdot g^{-1} \cdot min^{-1}$, representing a 26.42% increase compared to the control (Figure 11(a)). Concurrently, the NADH/NAD^+ ratio increased to 22.69 (Figure 10(a)), and ATP content peaked at 1.25 μmol/mg prot (Figure 9(a)). These results demonstrate that CO_3^{2-} enhances cytochrome c oxidase (Complex IV) functionality. This enhancement accelerates electron transfer from NADH to terminal acceptors, significantly elevating ATP synthesis and providing robust energy support for denitrification (Figure 12) [21,22]. Furthermore, CO_3^{2-} stabilizes denitrifying enzymes by coordinating with metal clusters in their active sites. At 200 mg/L CO_3^{2-}, NR activity increased by 55.15% (Figure 5(a)), while NiR activity rose by 50.44% (Figure 6(a)). The mechanism likely involves the strong coordination ability of CO_3^{2-}, which enables the formation of stable complexes with metal clusters (e.g., 4Fe-4S) in enzyme active sites. This interaction inhibits metal cluster oxidation and prevents enzyme conformational inactivation under high ion stress (Figure 13) [23]. Thus, CO_3^{2-}

enhances nitrogen removal rates in strain H6 through two pathways: Improving electron transfer efficiency and stabilizing enzyme structure.

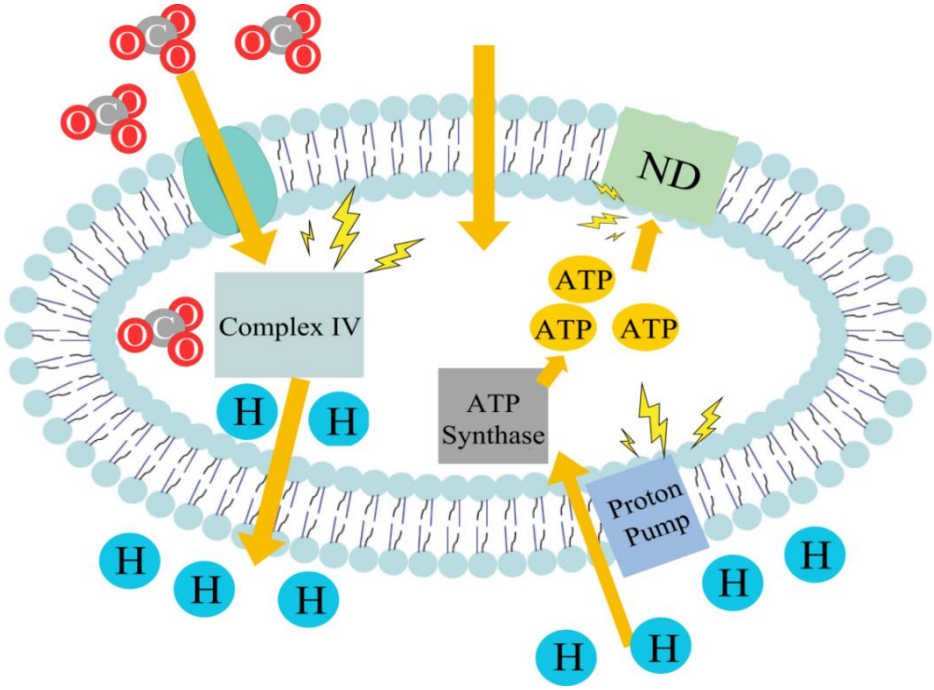

Figure 12. Schematic illustration of the enhancement of the electron transport chain and ATP synthesis by CO_3^{2-} during aerobic denitrification (notes: ATP: Adenosine triphosphate; Complex IV: cytochrome c oxidase; ND: Nitrification /De-Nitrification; and C-O: CO_3^{2-}).

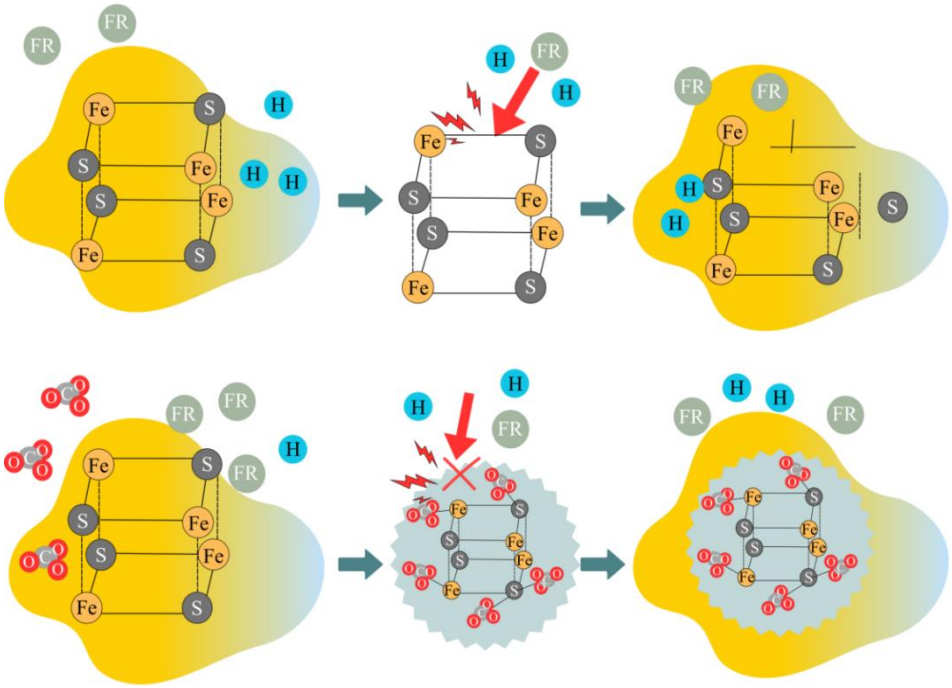

Figure 13. Proposed mechanism of CO_3^{2-} stabilizing the 4Fe-4S clusters in denitrification enzymes under high ionic stress (notes: FR: free radical; C-O: CO_3^{2-}; Fe: Iron; S: Sulfur; and Fe-S: [4Fe-4S] iron-sulfur cluster).

In contrast to the inhibitory effects of Cl^- and NO_3^-, and the limited role of HCO_3^-, the enhanced nitrogen removal by CO_3^{2-} results from two distinct yet synergistic mechanisms. First, CO_3^{2-} acts as an efficient intracellular pH buffer. It neutralizes protons (H^+) released during denitrification, thereby maintaining a stable, near-neutral microenvironment that supports optimal enzymatic activity [24]. In comparison, HCO_3^- shows weaker buffering capacity. This inadequacy leads to incomplete proton neutralization, resulting in suboptimal enzymatic performance [25,26]. Second, the high charge density of CO_3^{2-} promotes coordination with metal ions (e.g., Fe^{3+}) at enzyme active sites. This interaction facilitates the formation of stable complexes, which help protect redox-sensitive clusters such as [4Fe-4S] from oxidation or dissociation under ionic stress [23,27].

The experimental data provide strong evidence for this mechanistic comparison. At 200 mg/L, CO_3^{2-} achieved the highest NO_3^--N reduction rate (Figure 3(a)) and the most pronounced stimulation of intracellular electron transport system activity (ETSA) (Figure 11(a)). Its performance was consistently superior to that of HCO_3^-. Through the synergistic actions of pH regulation and enzyme stabilization, CO_3^{2-} systematically optimizes enhances electron transfer efficiency and cellular energy metabolism. Together, these effects drive the observed improvement in nitrogen removal.

Conversely, Cl^- and NO_3^- exhibited inhibitory effects at 200 mg/L. Moreover, NH_4^+-N removal decreased by 57.23% (Cl^-) and 67.19% (NO_3^-) compared to the control. Chloride likely disrupts membrane integrity through osmotic stress, impairing NADH dehydrogenase activity [28,29]. Nitrate competitively occupies the molybdenum cofactor-binding site in NarG, inducing feedback inhibition [30].

This study reveals the dual role of CO_3^{2-} as a metabolic enhancer, manifested through two mechanisms: (1) Maintaining a near-neutral microenvironment via alkalinity-driven H^+ buffering, and (2) stabilizing enzyme-metal interactions through its high charge density. Nevertheless, limitations persist. First, direct evidence of CO_3^{2-}-enzyme binding (e.g., via X-ray absorption spectroscopy or molecular docking) remains unresolved. Second, the regulatory mechanisms of narG and nirS genes under elevated CO_3^{2-} concentrations require further investigation. Additionally, the economic viability and operational of carbonate-buffered systems in wastewater treatment necessitate practical evaluation.

In conclusion, this work elucidates the pivotal role of alkaline ions in microbial metabolism and provides a theoretical foundation for low-carbon optimization of biological nitrogen removal processes. In future studies, researchers should focus on multi-ion interaction effects [31] and the application potential of CO_3^{2-} as a targeted metabolic modulator in complex environmental matrices.

5. Conclusions

This study demonstrates that CO_3^{2-} significantly enhances the nitrogen removal performance of the aerobic denitrifying bacterium H6 by synergistically optimizing the function of the electron transport chain and improving the stability of key denitrification enzymes. This finding challenges the conventional understanding that high ion concentrations exert inhibitory effects, and advances the knowledge on the regulatory role of alkaline ions in microbial metabolism. The findings of this study provide theoretical insight and practical guidance for the cost-effective biological treatment of high-ammonia nitrogen wastewater within carbonate-buffered, moderately high-salinity systems. Their applicability to other types of saline wastewater (e.g., those containing heavy metals or high sulfate) requires further validation. Thus, researchers should focus on elucidating the molecular mechanisms underlying this regulation and conducting pilot-scale validation to accelerate the translation of laboratory findings into engineering applications.

Use of AI tools declaration

The authors declare they have not used Artificial Intelligence (AI) tools in the creation of this article.

Acknowledgments

The authors gratefully acknowledge the financial support from the Henan Provincial Department of Science and Technology (262102320207) and the Nanyang Normal University Cultivation Project of the National Natural Science Foundation of China (2023PY021).

Conflict of interest

All authors declare no conflicts of interest in this paper.

References

1. Li X, Jin Y X, He YY, et al. (2025) Mechanisms of N_2O production in salinity-adapted partial nitritation systems for high-ammonia wastewater treatment. *Water Res X* 27: 100311. https://doi.org/10.1016/J.WROA.2025.100311
2. Wei R, Hui C, Zhang YP, et al. (2020) Nitrogen removal characteristics and predicted conversion pathways of a heterotrophic nitrification-aerobic denitrification bacterium, Pseudomonas aeruginosa P-1. *Environ Sci Pollut R* 28: 7503–7514. https://doi.org/10.1007/s11356-020-11066-7
3. Chen JL, Xu J, Zhang SN, et al. (2021) Nitrogen removal characteristics of a novel heterotrophic nitrification and aerobic denitrification bacteria, Alcaligenes faecalis strain WT14. *J Environ Manag* 282: 111961. https://doi.org/10.1016/J.JENVMAN.2021.111961
4. Song T, Zhang XL, Li J, et al. (2021) A review of research progress of heterotrophic nitrification and aerobic denitrification microorganisms (HNADMs). *Sci Total Environ* 801: 149319. https://doi.org/10.1016/J.SCITOTENV.2021.149319
5. Huang MQ, Cui YW, Huang JL, et al. (2022) A novel Pseudomonas aeruginosa strain performs simultaneous heterotrophic nitrification-aerobic denitrification and aerobic phosphate removal. *Water Res* 221: 118823. https://doi.org/10.1016/J.WATRES.2022.118823
6. Xi HP, Zhou XT, Arslan M, et al. (2022) Heterotrophic nitrification and aerobic denitrification process: Promising but a long way to go in the wastewater treatment. *Sci Total Environ* 805: 150212. https://doi.org/10.1016/J.SCITOTENV.2021.150212
7. Hou M, Li W, Li H, et al. (2019) Performance and bacterial characteristics of aerobic granular sludge in response to alternating salinity. *Int Biodeter Biodegr* 142: 211–217. https://doi.org/10.1016/j.ibiod.2019.05.007
8. Chen AL, Su X, Xing ZL, et al. (2022) Effect mechanism of individual and combined salinity on the nitrogen removal yield of heterotrophic nitrification-aerobic denitrification bacteria. *Environ Res* 214: 113834. https://doi.org/10.1016/J.ENVRES.2022.113834
9. Ma TF, Ma HX, Xing CY, et al. (2025) Physiological and proteomic insights into silver nanoparticle-induced stress responses and resistance mechanisms in aerobic denitrifying Enterobacter cloacae HNR. *J Environ Chem Eng* 13: 115934. https://doi.org/10.1016/J.JECE.2025.115934

10. Yin C, Li Y, Zhang TY, et al. (2020) Effects of exposure to anionic surfactants (SDBS and SDS) on nitrogen removal of aerobic denitrifier. *Water Environ Res* 92: 2129–2139. https://doi.org/10.1002/wer.1384
11. Shi CY, Gou F, Chen LA, et al. (2024) Influence and mechanism of typical transition metal ions on the denitrification performance of heterotrophic nitrification-aerobic denitrification bacteria. *Environ Res* 258: 119460. https://doi.org/10.1016/J.ENVRES.2024.119460
12. Fang JK, Liao SA, Zhang SS, et al. (2021) Characteristics of a novel heterotrophic nitrification-aerobic denitrification yeast, Barnettozyma californica K1. *Bioresource Technol* 339: 125665. https://doi.org/10.1016/J.BIORTECH.2021.125665
13. Wu GY, Yang GF, Sun XR, et al. (2023) Simultaneous denitrification and organics removal by denitrifying bacteria inoculum in a multistage biofilm process for treating desulfuration and denitration wastewater. *Bioresource Technol* 388: 129757. https://doi.org/10.1016/J.BIORTECH.2023.129757
14. Gao J, Duan XD, O'Shea K, et al. (2019) Degradation and transformation of bisphenol A in UV/Sodium percarbonate: Dual role of carbonate radical anion. *Water Res* 171: 115394. https://doi.org/10.1016/j.watres.2019.115394
15. Keykha HA, Zangani A, Romiani HM, et al. (2023) Characterizing microbial and CO_2-induced carbonate minerals: Implications for soil stabilization in sandy environments. *Minerals* 13: 976. https://doi.org/10.3390/MIN13070976
16. Shi LD, Gao TY, Wei XW, et al. (2022) pH-dependent hydrogenotrophic denitratation based on self-alkalization. *Environ Sci Technol* 57: 685–696. https://doi.org/10.1021/ACS.EST.2C05559
17. Fernández AR, Areias C, Daffonchio D, et al. (2022) The role of microorganisms in the nucleation of crbonates, environmental implications and applications. *Minerals* 12: 1562. https://doi.org/10.3390/MIN12121562
18. Yue X, You A, Liu Y, et al. (2023) Low-concentration methanol effect on the microorganisms, nitrogen removal, and recovery of the completely autotrophic nitrogen removal over nitrite. *Water Sci Technol* 87: 130–143. https://doi.org/10.2166/WST.2022.417
19. Hu T, Wei JT, Ding YH, et al. (2024) Characterisation of Pseudomonas mosselii H6 for aerobic denitrification: Stoichiometry and reaction kinetics. *Biotechnol Biotec Eq* 38. https://doi.org/10.1080/13102818.2024.2402445
20. Zhang Y, Bao JG, Du JK, et al. (2023) Comprehensive metagenomic and enzyme activity analysis reveals the inhibitory effects and potential toxic mechanism of tetracycline on denitrification in groundwater. *Water Res* 247: 120803. https://doi.org/10.1016/J.WATRES.2023.120803
21. Chen JH, Xue Y, Yang DL, et al. (2023) Optimizing waste molasses utilization to enhance electron transfer via micromagnetic carriers: Mechanisms and high-nitrate wastewater denitrification performance. *Environ Res* 242: 117709. https://doi.org/10.1016/J.ENVRES.2023.117709
22. Yang G, Luo YD, Bian YH, et al. (2024) Electro-mediated cathodic oxygen drives respiration chain electron transfer of electroactive bacteria to enhance refractory organic biological oxidation. *Water Res* 268: 122585. https://doi.org/10.1016/J.WATRES.2024.122585
23. Feng J, Shaik SS, Wang BJ (2021) Spin-regulated electron transfer and exchange-enhanced reactivity in Fe_4S_4-mediated redox reaction of the Dph_2 enzyme during the biosynthesis of Diphthamide. *Angew Chem Int Edit* 60: 20430–20436. https://doi.org/10.1002/anie.202107008
24. Huang JE, Li FW, Ozden A, et al. (2021) CO_2 electrolysis to multicarbon products in strong acid. *Science* 372: 1074–1078. https://doi.org/10.1126/SCIENCE.ABG6582

25. Zhang ZS, Gao PT, Guo L, et al. (2020) Elucidating temperature on mixotrophic cultivation of a Chlorella vulgaris strain: Different carbon source application and enzyme activity revelation. *Bioresource Technol* 314: 123721. https://doi.org/10.1016/j.biortech.2020.123721
26. Marcandalli G, Boterman K, Koper M (2022) Understanding hydrogen evolution reaction in bicarbonate buffer. *J Catal* 405: 346–354. https://doi.org/10.1016/J.JCAT.2021.12.012
27. Lan QF, Yang YM, Xie ZY, et al. (2023) Molecular dynamics calculation of the coordination behavior of Yb (III) in Sodium Carbonate solution. *Processes* 11: 2624. https://doi.org/10.3390/PR11092624
28. Jentsch TJ, Pusch M (2018) CLC Chloride channels and transporters: Structure, function, physiology, and disease. *Physiol Rev* 98: 1493–1590. https://doi.org/10.1152/physrev.00047.2017
29. Yoshinori M (2023) Physiological roles of chloride ions in bodily and cellular function. *J Physiol Sci* 73: 31. https://doi.org/10.1186/S12576-023-00889-X
30. Wang H, Lu HG, Xu L, et al. (2021) Molybdate transporter ModABC contributes to Klebsiella pneumoniae muscle infection and new insight into its treatment. *Microbiology* 48: 2784–2800. https://doi.org/10.13344/j.microbiol.china.201103
31. Peters K, Staehlke S, Rebl H, et al. (2024) Impact of metal ions on Cellular functions: A focus on mesenchymal stem/stromal cell differentiation. *Int J Mol Sci* 25: 10127. https://doi.org/10.3390/IJMS251810127